Received: 18 February 2021 | Revised: 12 May 2021 | Accepted: 21 June 2021

DOI: 10.1002/mp.15084

RESEARCH ARTICLE

MEDICAL PHYSICS

Motion artifacts assessment and correction using optical tracking in synchrotron radiation breast CT

Luca Brombal[1,2] | **Lucia Mariel Arana Peña**[1,2] | **Fulvia Arfelli**[1,2] | **Renata Longo**[1,2] | **Francesco Brun**[2,3] | **Adriano Contillo**[4] | **Francesca Di Lillo**[4] | **Giuliana Tromba**[4] | **Vittorio Di Trapani**[5,6] | **Sandro Donato**[7,8] | **Ralf Hendrik Menk**[2,4,9] | **Luigi Rigon**[1,2]

[1]Department of Physics, University of Trieste, Trieste, Italy

[2]Division of Trieste, Istituto Nazionale di Fisica Nucleare, Trieste, Italy

[3]Department of Engineering and Architecture, University of Trieste, Trieste, Italy

[4]Elettra-Sincrotrone Trieste S.C.p.A., Trieste, Italy

[5]Department of Physical sciences, Earth and environment, University of Siena, Siena, Italy

[6]Division of Pisa, Istituto Nazionale di Fisica Nucleare, Pisa, Italy

[7]Department of Physics, University of Calabria, Arcavacata di Rende, Cosenza, Italy

[8]Division of Frascati, Istituto Nazionale di Fisca Nucleare, Frascati, Rome, Italy

[9]Department of Medical Imaging, University of Saskatchewan, Saskatoon, Canada

Correspondence
Francesco Brun, Department of Engineering and Architecture, University of Trieste, via Valerio 6/1, 34127 Trieste, Italy.
Email: fbrun@units.it

Funding information
Open Access Funding provided by Universita degli Studi di Trieste within the CRUI-CARE Agreement.

Abstract

Purpose: The SYRMA-3D collaboration is setting up a breast computed tomography (bCT) clinical program at the Elettra synchrotron radiation facility in Trieste, Italy. Unlike the few dedicated scanners available at hospitals, synchrotron radiation bCT requires the patient's rotation, which in turn implies a long scan duration (from tens of seconds to few minutes). At the same time, it allows the achievement of high spatial resolution. These features make synchrotron radiation bCT prone to motion artifacts. This article aims at assessing and compensating for motion artifacts through an optical tracking approach.

Methods: In this study, patients' movements due to breathing have been first assessed on seven volunteers and then simulated during the CT scans of a breast phantom and a surgical specimen, by adding a periodic oscillatory motion (constant speed, 1 mm amplitude, 12 cycles/minute). CT scans were carried out at 28 keV with a mean glandular dose of 5 mGy. Motion artifacts were evaluated and a correction algorithm based on the optical tracking of fiducial marks was introduced. A quantitative analysis based on the structural similarity (SSIM) index and the normalized mean square error (nMSE) was performed on the reconstructed CT images.

Results: CT images reconstructed through the optical tracking procedure were found to be as good as the motionless reference image. Moreover, the analysis of SSIM and nMSE demonstrated that an uncorrected motion of the order of the system's point spread function (around 0.1 mm in the present case) can be tolerated.

Conclusions: Results suggest that a motion correction procedure based on an optical tracking system would be beneficial in synchrotron radiation bCT.

KEYWORDS
breast CT, motion artifacts, optical tracking, phase contrast

1 | INTRODUCTION

Breast computed tomography (bCT) is an x-ray technique emerging in clinical practice and, in recent years, several dedicated studies describing different setups and involving an increasing number of patients have been published.[1-7] three-dimensional (3D) imaging of the breast allows the reduction of anatomical noise and masking effects inherent to two-dimensional mammography, and it is regarded as a valuable tool to improve early detection of breast cancer, follow-up, and treatment/surgery planning stages. Additionally, bCT does not require breast compression, thus entirely avoiding patient discomfort. In fact, more than 50% of women experience moderate to extreme discomfort during mammography,[8] even discouraging some from the participation in the screening program.[9] On the other hand, bCT is an extremely demanding imaging task as tomographic data must provide both high spatial resolution, to identify microcalcifications, and high contrast resolution, to distinguish between soft tissues composing the breast. This must be attained with a low delivered radiation dose (i.e., few milligrays), as imposed by regulatory bodies due to breast radiosensitivity. While these conflicting requirements certainly slowed down widespread use of bCT in clinical practice, many improvements have been recently introduced leading to a new generation of bCT systems based on a fan-shaped x-ray beam and photon-counting detectors.[10] At the same time, two research groups, working, respectively, at the Italian synchrotron facility Elettra (Trieste, Italy)[11-13] and at the ANSTO Australian Synchrotron (Melbourne, Australia),[14,15] are developing clinical programs to scan patients with synchrotron radiation making use of x-ray phase-contrast imaging (XPCi) techniques.[16,17] The main advantage of synchrotron radiation stems from the high degree of coherence, both temporal and spatial, of the x-ray beam. The first permits a monochromatic beam whose energy can be tuned depending on the sample size and composition to optimize the signal-to-noise ratio at a given radiation dose.[18,19] The latter enables a straightforward implementation of the propagation-based XPCi. In this technique an imaging detector, positioned at a given (propagation) distance downstream from the sample, records the near-field interference pattern due to the phase-shift accumulated by the x-rays across the imaged object.[20] Images obtained in this configuration, which show an additional contrast, or edge enhancement, arising at the interfaces between different materials, are further processed via a so-called phase-retrieval filter.[21] The final result of this imaging chain is a substantial decrease in image noise at the same contrast and spatial resolution levels that would be observed in a conventional x-ray attenuation-based tomography.[22,23]

In this framework, the presence of patients' motion-related artifacts and their impact on the diagnostic significance of the examination is still an open issue and, to the best of the authors' knowledge, no dedicated studies have been published to date. In fact, the absence of the compression paddles which constrain the breast in a fixed position makes bCT images more prone to artifacts due to patient movements, both voluntary and involuntary (e.g., breathing). In principle, these effects are more critical in synchrotron-based than in hospital-based bCT setups for two reasons. First, the scan duration is generally longer at synchrotrons (from tens of seconds to few minutes) as the patient must be rotated instead of the x-ray source, thus limiting the rotation speed to velocities in the order of 10 degrees per second. This may prevent the possibility of a breath-holding examination and increases the probability of patient movement. Second, synchrotron bCT systems generally feature a better spatial resolution, up to 7 lp/mm at 10% of the modulation transfer function, or ~0.1 mm at full width at half maximum (FWHM) of the point spread function,[24] being more sensitive to small displacements. To mitigate these effects, the usefulness of dedicated breast immobilizer systems, both for conventional and synchrotron-based setups, has been proposed[25,26] but, at present, such systems are seldom used in clinical practice.

In this context, the study here presented has been conceived for three purposes. First, to develop a simple model for the respiratory motion by evaluating real breathing displacements on seven volunteers with optical tracking. Second, to evaluate the effect of such modeled motion on reconstructed tomographic images of a breast phantom and a surgical specimen. Lastly, to introduce a correction method to compensate for the resulting artifacts. Although data-driven techniques based on refined image registration approaches have been proposed for motion compensation in tomographic imaging,[27-30] the use of external hardware to implement an optical tracking system is here suggested and discussed.

All the presented activities have been carried out in the framework of the SYRMA-3D collaboration,[12,31] which is conducting a comprehensive study on synchrotron-based bCT, including *ad-hoc* Monte Carlo simulation software for dose evaluation,[32,33] modeling of the whole imaging chain,[34,35] dedicated reconstruction algorithms,[36-38] and image quality assessment procedures.[39]

2 | MATERIALS AND METHODS

2.1 | Synchrotron radiation breast CT

The SYRMA-3D collaboration is setting up a clinical bCT facility at the SYRMEP beamline at Elettra,[40] utilizing the same patient room which hosted the XPCi

planar mammography clinical study.[41] The geometry of the bCT system requires that the patient lies prone on a horizontal, ergonomically designed, high-precision support (CINEL Strumenti Scientifici s.r.l.), which is capable of rotating around the vertical axis, as well as translating horizontally and vertically (see Figure 1). The patient's support features a central aperture, whereby the pendant breast can be scanned through the laminar x-ray beam. A full volume acquisition is obtained via subsequent 180-degree scans performed at different vertical positions,[42] each of a duration of 40 s or less, resulting in an expected total examination time of 5 to 10 min. According to breast dimension and glandularity, the x-ray energy is selected between 25 and 30 keV,[43] with a target mean glandular dose delivery of 5 mGy or less. A detailed description of this bCT project was recently reported.[12]

2.2 | Patient's motion preliminary assessment

To evaluate the patient's motion, a preliminary assessment has been performed on seven female volunteers. The volunteers were not exposed to x-rays but were simply asked to lie prone on the support in the patient's position, and to let their left breast dangle in a pendant geometry outside of the central aperture. The left breast was chosen because it was assumed that it might be more directly affected by involuntary heartbeat-related movements. To estimate the movements, a white band with a fine pen black dot was applied to the dangling breast of each volunteer and images of this fiducial mark were acquired with an optical camera (Basler acA1920-155um equipped with a Kowa LM25HC 25 mm lens with an F 1.4-16 iris range). The optical camera was positioned at the same height as the fiducial mark, at a distance of about 50 cm from the sample, and was used to record 400 frames of the fiducial mark in 40 s (10 Hz frame rate), corresponding to the duration of a single scan. The volunteers were instructed to relax and to breathe normally. After manually selecting a region of interest (ROI) suitable for all frames, a mask corresponding to the fiducial mark was obtained for each frame by performing a single global threshold segmentation. Hence, the fiducial mark position was obtained by calculating the center of mass (CoM) coordinates of the masked pixels. Finally, calibration in millimeter units was performed by means of a reference image. The movements of the fiducial mark were assumed to yield a coarse estimation of a typical patient's breast movement.

2.3 | Imaging setup

The tomographic images presented in this study were acquired in the experimental room, which is located upstream of the room which hosts the patient's support. Here, a set of high-precision motor stages allows the combination of translational and rotational motions. A simplified sketch of the experimental setup is shown in Figure 2a. The x-ray source is a storage ring bending magnet generating a highly collimated polychromatic beam (vertical divergence of 0.2 mrad, horizontal divergence of 7 mrad). The beam is monochromatized by means of a Si(111) double-crystal monochromator, allowing the selection of energy in the range 8.5–40 keV with an effective resolution of around 0.1%. The beam cross-section at the sample, positioned at 22.5 m from the source, is 150 mm (horizontal) × 5 mm (vertical). Owing to the implementation of a dedicated beam-flattening filter, the otherwise Gaussian vertical intensity distribution is nearly constant, leading to uniform dose and signal-to-noise ratio distributions across the sample.[44] The x-ray flux is monitored through a custom ionization chamber positioned upstream of the sample stage (Figure 2b).

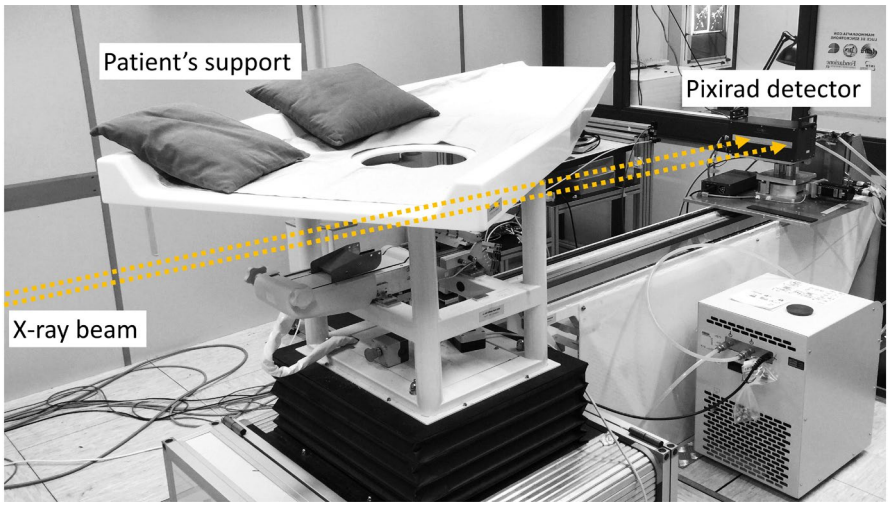

FIGURE 1 Image of the patient room at the SYRMEP beamline [Color figure can be viewed at wileyonlinelibrary.com]

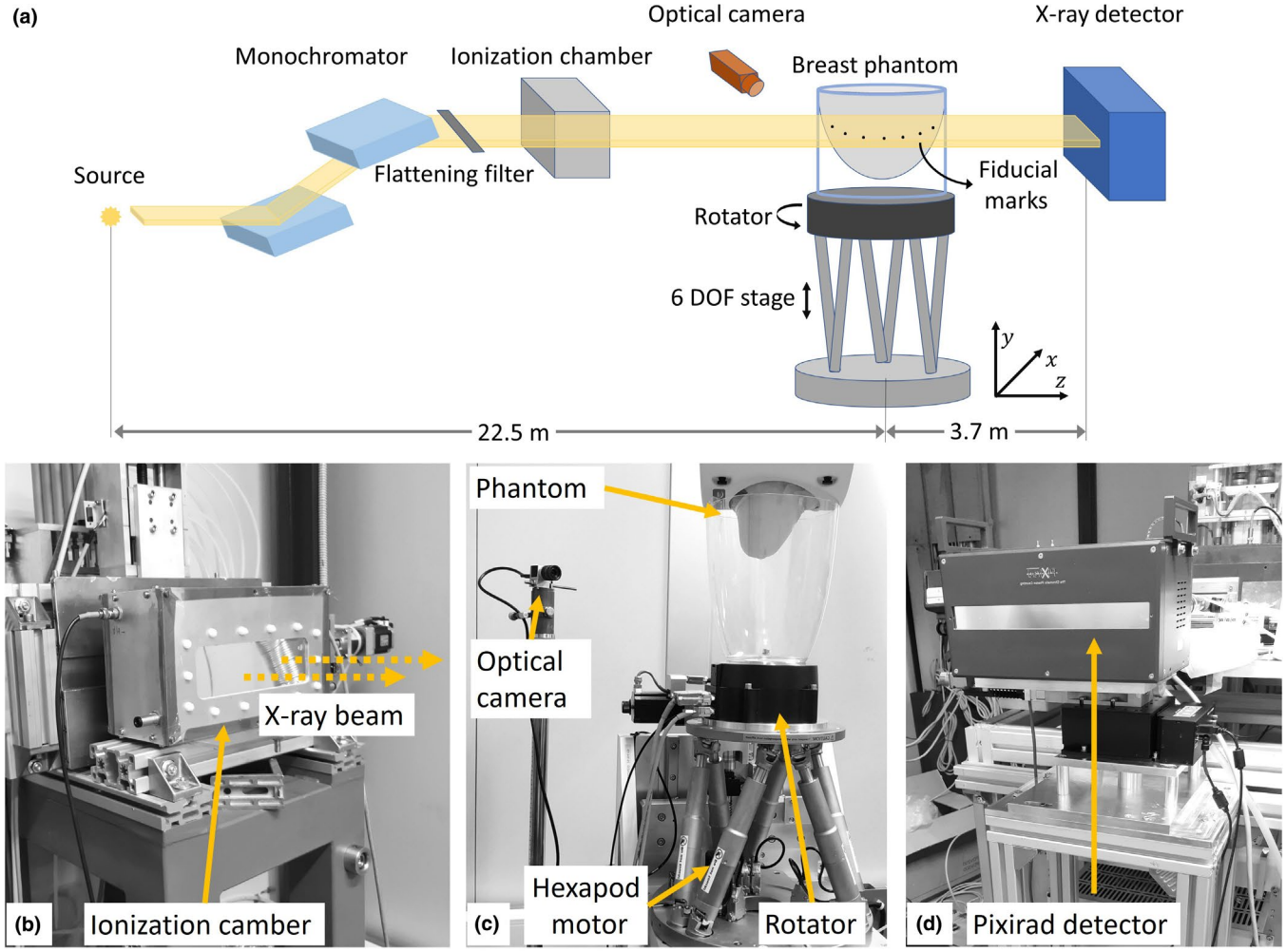

FIGURE 2 Sketch of the experimental setup (a) and related images of the ionization chamber (b), sample stage (c), and detector (d) [Color figure can be viewed at wileyonlinelibrary.com]

Samples are positioned on a high-precision rotator (Micos UPR-160 Air) spinning at 4.5 deg/s, corresponding to an angular interval of 0.15 degrees per projection. The rotator is mounted on a programmable six degrees of freedom (DOF) hexapod positioning stage (Physik Instrumente H-840.G2), which was programmed to simulate breathing-induced oscillations (Figure 2c). In principle, the hexapod positioning stage can execute complex trajectories; however, for the sake of simplicity and taking into account the preliminary evaluation of the respiratory motion on the volunteers in prone position (reported in Section 3.1), only vertical oscillations were simulated since they are dominant over the horizontal ones. In particular, a periodic oscillatory motion with constant speed, amplitude of 1 mm, and frequency of 12 cycles/minute was programmed and was superimposed upon sample rotation during the tomographic acquisition. To monitor the motion, motor positions were logged at a rate of 30 Hz, ensuring a good match with the sampling of tomographic projections.

The imaging device is a large-area photon-counting detector (Pixirad-8), based on a 650 μm thick CdTe sensor bump bonded on the readout ASIC,[45,46] and it is shown in Figure 2d. The readout electronics is optimized to obtain a negligible dead time between consecutive frames, allowing continuous acquisition without losing counts. The detector is assembled from eight modules, tiled to a global active area of 246 mm × 24.8 mm, while pixels are arranged on a honeycomb array with a 60 μm pitch, corresponding to a matrix of 4096 × 476 pixels. The detector is positioned 3.7 m downstream from the sample stage, enabling propagation-based XPCi, and it is operated at its maximum frame rate of 30 Hz, resulting in 1200 equally spaced projection images acquired over the 180-degree rotation of the sample.

2.4 | Scanned samples

Two samples were scanned with x-rays for this study. The first is a surgical breast specimen, with dimensions of 140 mm × 20 mm × 90 mm containing a moderate-grade ductal infiltrating carcinoma with a maximum

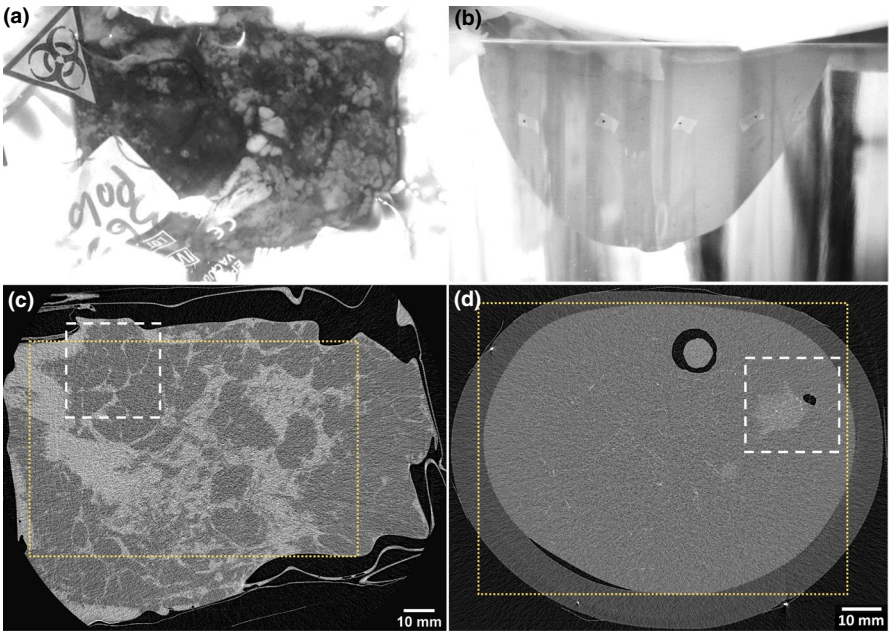

FIGURE 3 Images of the breast specimen sealed in the vacuum bag (a), of the breast phantom captured with the camera used for optical tracking (b), and their respective ground truth motionless tomographic reconstructions (c,d). White dashed boxes indicate the magnified regions shown in Figures 7 and 9, yellow dotted boxes indicate the regions used to evaluate SSIM and nMSE in Figures 8 and 10, respectively. The content of panels (c,d) is detailed in Section 2.6 [Color figure can be viewed at wileyonlinelibrary.com]

diameter of 35 mm. Before the scan, the sample was formalin-fixed and sealed in a vacuum bag, as shown in Figure 3a. The sample was handled following the Directive 2004/23/EC of the European Parliament and of the Council of 31 March 2004 on setting standards of quality and safety for the donation, procurement, testing, processing, preservation, storage, and distribution of human tissues. XPCi was performed within the framework of the operative protocol of the Breast Unit of the Trieste University Hospital ("PDTA Neoplasia mammaria" approved on 11 December 2019 by ASUGI–Azienda Sanitaria Universitaria Giuliana Integrata, Italy). The protocol entails a written informed consent which is obtained from the patients before their inclusion into bCT imaging studies. The specialist breast center of ASUGI is in compliance with the standard of EUSOMA guidelines (certificate No. 1027/01). In the study at hand, the images of the specimen were used to assess the magnitude of artifacts due to different degrees of uncompensated motion on a real breast tissue texture.

The second sample is a multi-modality breast phantom (CIRS model 073), shown in Figure 3b, simulating the breast shape, feel, and appearance for x-ray, ultrasound, and MRI imaging. The phantom mimics the presence of cystic dense lesions embedded in a homogeneous background and contains several microcalcifications with diameters ranging between 100 and 300 μm. To simulate the clinical examination, the phantom was imaged in a pendant geometry. To track the motion of the phantom, 16 equally spaced fiducial marks were applied on its surface to allow easy segmentation and image analysis in the optical tracking procedure. During the irradiation, the fiducial marks were imaged with the same optical camera previously described, which was positioned perpendicularly to the x-ray propagation direction (z) at the same height of the fiducial marks and a distance of about 50 cm from the sample. The frame rate of the camera was set to 30 Hz to match the x-ray detector's frame rate, while its gain was optimized to ensure the best visibility of the fiducial marks used for tracking. It should be noted that, differently from the preliminary motion estimation on the volunteers, the displacements are here assessed by tracking multiple fiducial marks as the sample is rotating while the camera is at a fixed position. Both samples were scanned at 28 keV at an entrance air kerma of 10 mGy, corresponding to a mean glandular dose of 5 mGy, which is comparable to values used in clinical practice. Details of the conversion between the entrance air kerma and the mean glandular dose can be found in appropriate publications.[12,32,33]

2.5 | Optical tracking

The goal of the tracking procedure is to follow the motion of the fiducial marks yielding, for each projection, the displacement of the sample along the vertical axis. For this purpose, a small ROI is selected in the center of each frame to minimize parallax errors. As schematically shown in Figure 4, the cropped image grayscale is then inverted (a) and segmented (b) by using a single global threshold providing a mask corresponding to the reference mark. The position of the mark is identified by the CoM coordinates of the masked pixels (c). Since the sample is rotating, the procedure must track many consecutive marks moving in front of the camera. To this end, when the tracked point falls outside the selected ROI, the

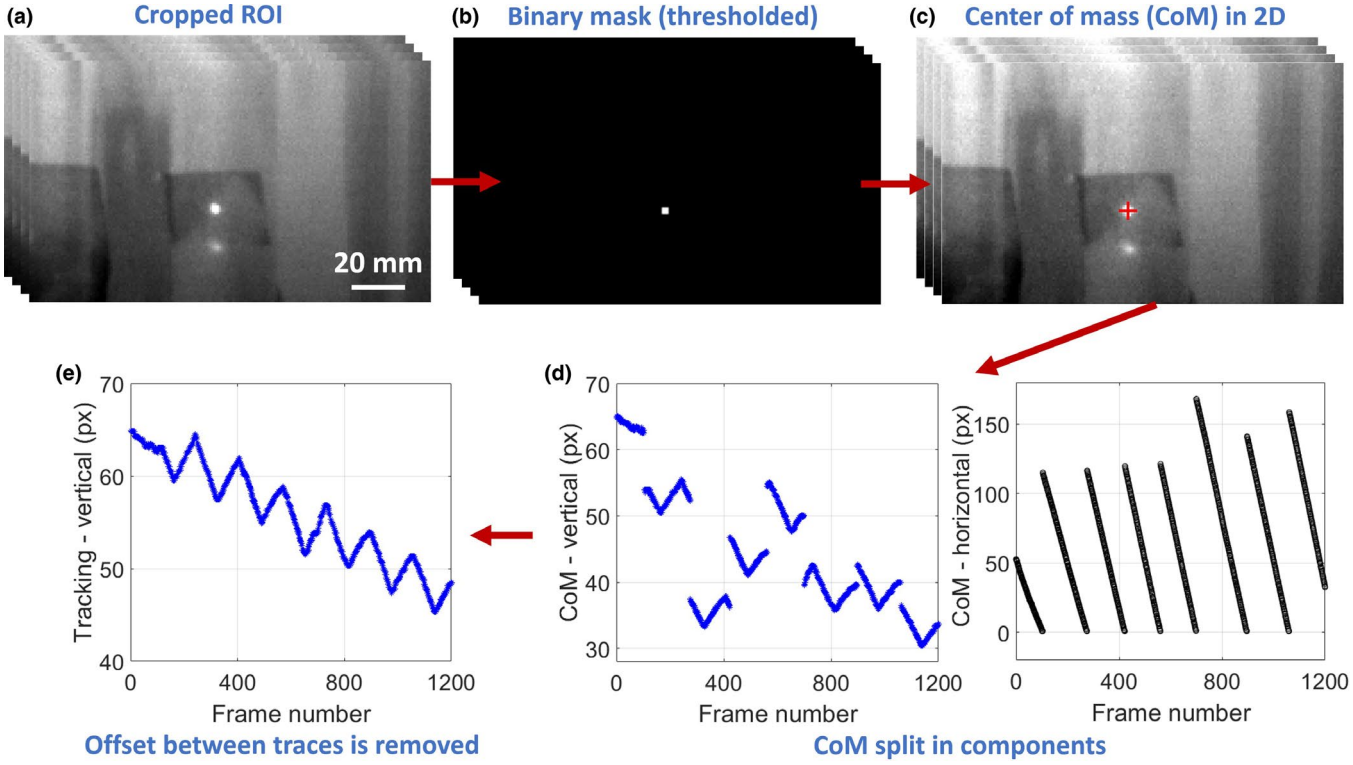

FIGURE 4 Diagram of the optical tracking procedure. The individual steps are discussed in the main text [Color figure can be viewed at wileyonlinelibrary.com]

procedure seeks the next one and starts tracking it (see Movie S-1). In this way, the final tracks, along both vertical and horizontal directions, will be composed of many sub-tracks, each corresponding to a different mark (d). At this point, the sub-tracks along the vertical direction are joined together by removing the offset between each sub-track pairs, yielding a single continuous displacement track (e). It should be noted that the linear trend which can be observed in the final track is due to a slight tilt of the camera with respect to the rotation plane, which can be estimated to be below 1 degree. As will be clear in the following, this trend can be easily compensated via linear fitting and it does not impair the procedure's results. In order to test the reliability of the optical tracking system, and to perform an initial calibration, a reference dataset tracked without moving the hexapod stage has been generated and the resulting track has been subtracted from the motion track as shown in Figure 5a-c. The subtraction in panel (c) correctly reproduces the programmed oscillatory motion, carried out at constant speed over an amplitude of 1 mm, and it can be matched to the actual motor positions. Thus, by tracking the motion of a simple object, which is displaced by a known length, a calibration factor to convert the tracked displacements from pixels to millimeters is obtained. Of note is that this is a one-time calibration procedure. Once the optical system is calibrated, the raw tracking data previously obtained [panel (d), also previously reported in Figure 4e] are treated with a linear fit de-trending procedure (e), and the calibration factor is applied. In this particular case, it can be verified that the corrected and calibrated trajectory accurately reproduces the actual motor positions (f).

2.6 | Image processing and analysis

Raw tomographic data streamed from the detector are firstly pre-processed via a dedicated procedure coping with detector-specific artifacts, such as charge trapping, which is often encountered when using high-Z sensors.[47] Following the pre-processing, the phase-retrieval filter is applied to projection images. At this stage, projections are translated to compensate for the vertical motion imposed during the acquisition. In the case of the breast specimen sample, images are corrected based on the actual motor position tracks. For this sample no optical tracking procedure has been implemented due to its rather unrealistic surface shape and volume, and to the presence of the vacuum bag wrapping the specimen. Specifically, six datasets are generated with different projection translation amplitudes, that is, by leaving various degrees of uncompensated motion: one dataset takes into

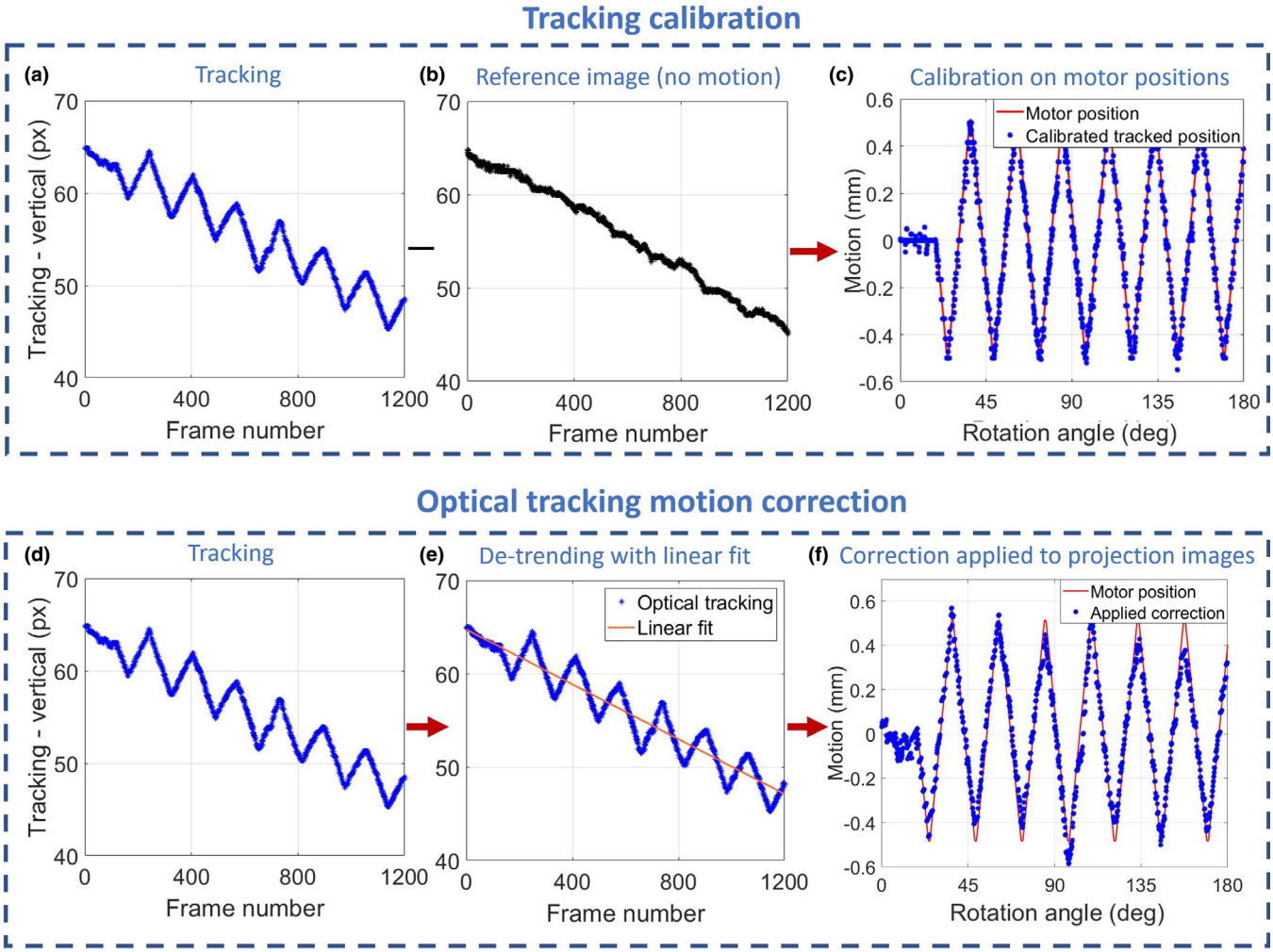

FIGURE 5 Diagrams of the tracking calibration procedure, from (a) to (c), and of the procedure to obtain the final correction to be applied to projection images, from (d) to (f) [Color figure can be viewed at wileyonlinelibrary.com]

account the full motor displacement, while the other are under-corrected, leaving 0.05, 0.1, 0.2, 0.5, and 1 mm (no correction) of residual motion, respectively. In this way, datasets with different displacements are virtually simulated. Conversely, for the breast phantom data, the translation of the projections is directly based on the optical tracking results. Also in this case, to evaluate the effectiveness and quality of the tracking procedure, both non-corrected and corrected based on motor positions datasets are generated. After motion compensation, each dataset is finally reconstructed via a GPU-based filtered back projection algorithm with a Shepp–Logan filter.[48] Owing to the small divergence of the beam, a parallel geometry is assumed in CT reconstruction. Considering the slight geometrical magnification, due to the propagation distance between sample and detector, and the detector's pixel arrangement, the reconstructed voxel size is 51.5 × 51.5 × 44.7 μ m^3.

To quantitatively assess the effects of motion and motion compensation procedures, the reconstructed images, both of the breast specimen and the phantom, are compared with reference images acquired without vertical motion. These ground truth tomographic slices are shown in panels (c) and (d) of Figure 3. The comparison is carried out by evaluating two similarity metrics that are well known in the field of image processing, namely the structural similarity (SSIM) index and the normalized mean square error (nMSE).[49] SSIM values vary between 0 and 1, with 1 indicating two identical images, while nMSE values are positive real numbers, with 0 indicating identical images. For each dataset, these metrics are evaluated on five adjacent slices, allowing the computation of their mean values and standard errors of the mean, which are reported in the plots in the results section. Results for the breast specimen are detailed in Section 3.2, whereas artifacts compensation results for the breast phantom are discussed in Section 3.3

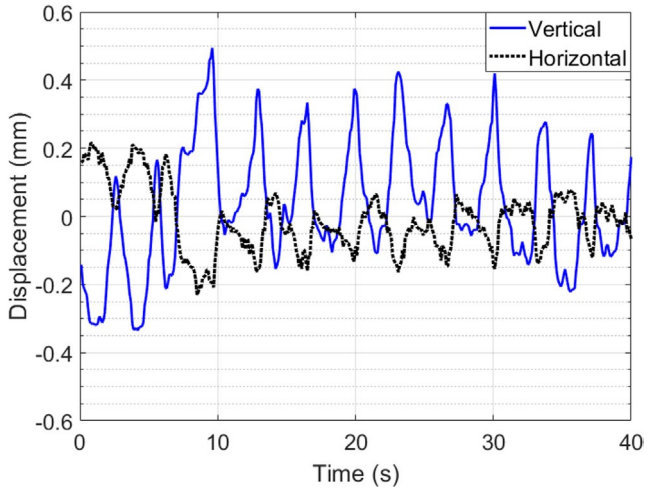

FIGURE 6 Optically tracked vertical and horizontal displacements on a volunteer's breast. The maximum displacements are 0.7 mm in the vertical direction and 0.4 mm in the horizontal direction [Color figure can be viewed at wileyonlinelibrary.com]

3 | RESULTS

3.1 | Assessment of motion on volunteers

Figure 6 displays representative tracks of vertical and horizontal displacements optically tracked on a volunteer, lying prone on the patient's support and breathing normally: vertical motion (maximum displacement 0.7 mm, blue solid line) is prominent over horizontal motion (maximum displacement 0.4 mm, black dotted line). Overall, considering the recorded movements of the seven volunteers, typical oscillations in the range 0.4–1.0 mm were observed in the vertical direction and in the range 0.2–0.5 mm in the horizontal direction, with a frequency ranging from 9 to 18 cycles/minute.

3.2 | Impact of motion on CT images

Figure 7 displays a single detail containing a spiculated fibroglandular tissue component (bright) embedded

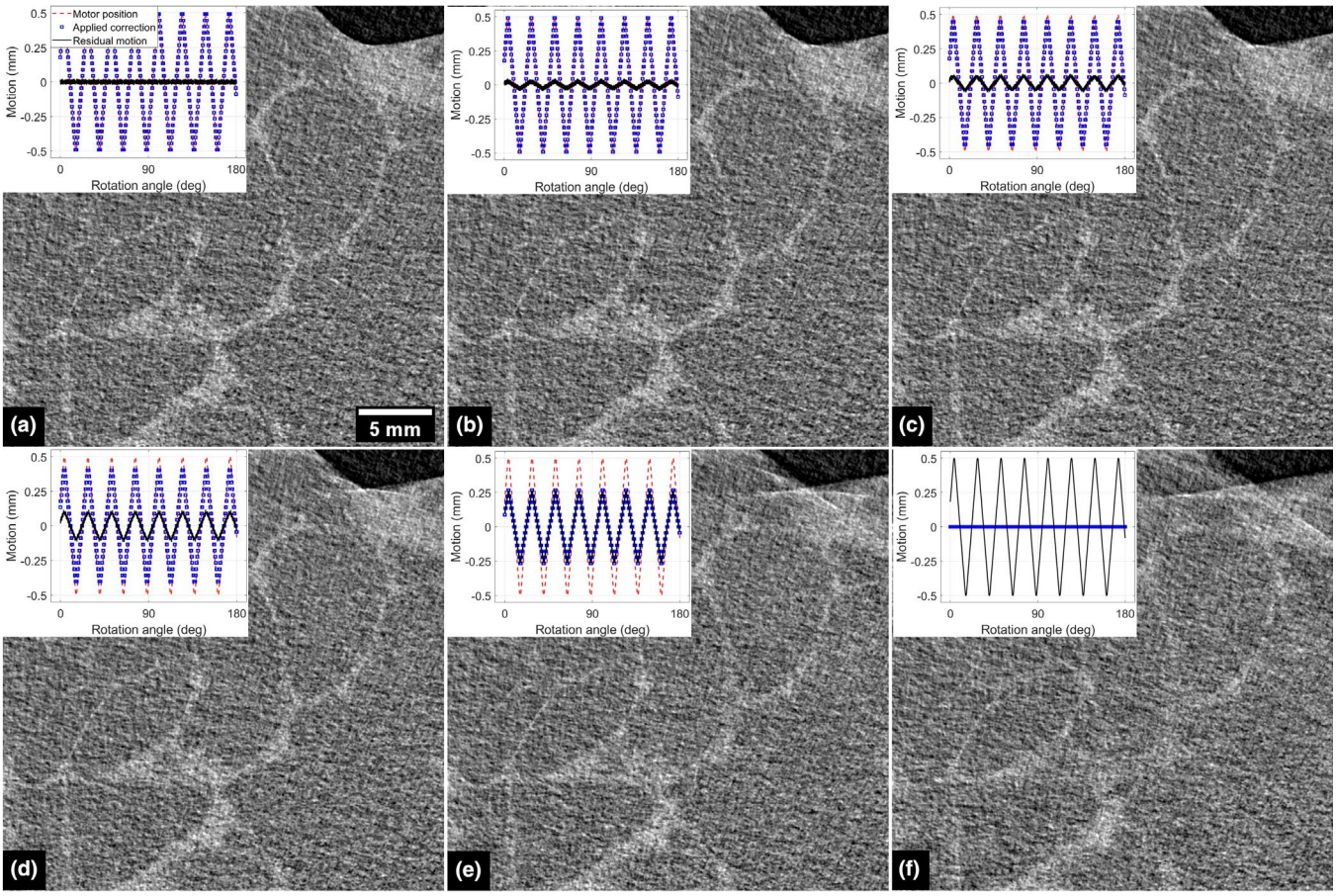

FIGURE 7 Detail of the breast specimen sample reconstructed compensating for the vertical motion (a), leaving a residual motion of 0.05, 0.1, 0.2, and 0.5 mm, from (b) to (e), and without any correction (f). The inset in each panel shows the actual motor positions (red dashed line), the applied correction for each projection (blue points), and the residual motion (solid black line) [Color figure can be viewed at wileyonlinelibrary.com]

in an adipose background (dark) as well as a sharp interface between tissue and air (black), which is reconstructed with different degrees of uncompensated motion as shown in the tracks reported in the insets.

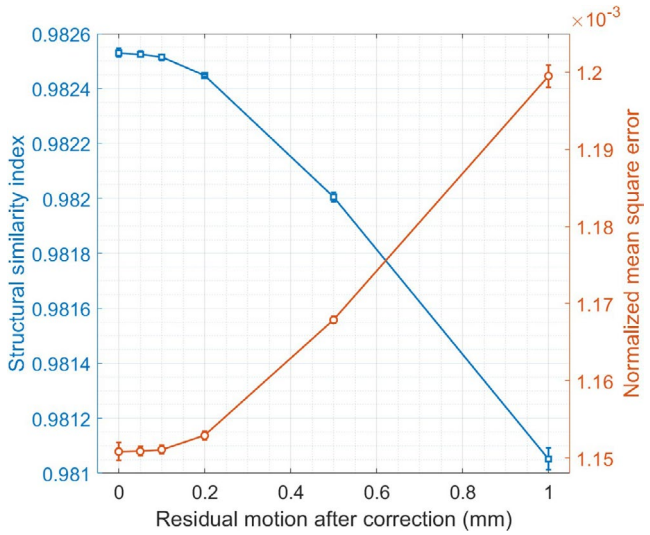

FIGURE 8 Plot displaying the structural similarity index (SSIM, blue curve and points) and the normalized mean square error (nMSE, orange curve and points) as a function of the residual vertical motion left after the correction. When not visible the error bars are smaller than the markers [Color figure can be viewed at wileyonlinelibrary.com]

Specifically, in panel (a) the image is reconstructed exactly compensating for motor movement, in panels (b) to (e) reconstructions include a residual motion of 0.05, 0.1, 0.2, and 0.5 mm, respectively, while in panel (f) no motion compensation is applied. From the images, it is clear that when no motion correction is applied the fibroglandular component is severely blurred and the visibility of connections is almost entirely lost. Additionally, artifacts arising at the boundary of the sample impair the visibility of the surrounding region and, more importantly, they propagate within the tissue, reducing the overall image quality. Similar considerations hold also in the case of the 0.5 mm residual motion amplitude, whereas artifacts become much less severe at 0.2 mm. For residual displacements of 0.1 and 0.05 mm, the differences with respect to the fully corrected image are almost negligible as the amount of residual motion is smaller than, or comparable to, the system's spatial resolution (i.e., ~0.1 mm at FWHM of the point spread function).

The presented qualitative visual assessment is supported by the quantitative results of Figure 8, where SSIM and nMSE, measured against the reference motionless image within the yellow dotted area in Figure 3c, are plotted as a function of the residual vertical displacement. From the plot it can be seen that both SSIM and nMSE present a plateau and, for each metric, data points are compatible with each other for residual motions below 0.1 mm, indicating

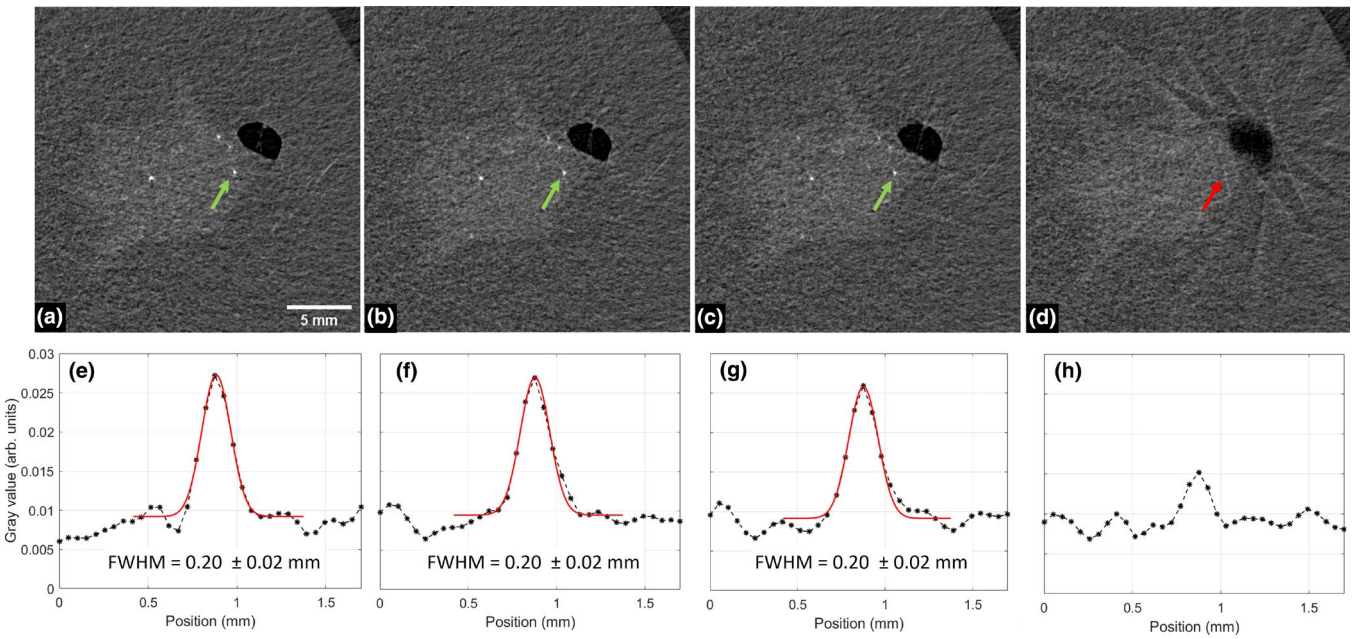

FIGURE 9 Detail of the breast phantom reconstructed from a reference motionless dataset (a), from the vertically displaced dataset corrected with the actual motor positions (b), with the optical tracking procedure (c), and without correction (d). In panels (e) to (h) the respective line profiles (black dots) and Gaussian fit (red line) across the microcalcification indicated with the arrow (green when visible and red when not visible). Uncertainties on the FWHM measurements are evaluated as the 95% confidence intervals of the fit parameters. Lines for the intensity profile evaluation are not shown in the figure in order not to mask the microcalcification [Color figure can be viewed at wileyonlinelibrary.com]

that these motions can be tolerated as they do not affect image quality. On the other hand, both curves have a steep dependence on the vertical displacement for motions larger than 0.2 mm, implying that in this range motion artifacts are critical and impact on image quality.

3.3 | Motion artifact compensation

The detail of the breast phantom shown in Figure 9 includes a simulated cystic lesion embedded in a breast tissue equivalent background. The lesion contains several microcalcifications, while in its periphery an air cavity can be observed. The latter feature, despite not being present in a real breast, is useful in determining the quality of the optical tracking correction since high-contrast interfaces (e.g., air/tissue) are sensitive to small displacements. Panels (a) to (d) show the static reference, the reconstruction corrected starting from the actual motor positions, corrected with the optical tracking and not corrected, respectively. Of note is that the correction based on motor position, which obviously is not feasible in a clinical scenario where the patient is moving freely, has been performed to quantify how far the optical tracking is from the case of a perfect motion-compensated dataset. From the figures it is clear that, if no motion correction is applied (d), the amount of blurring introduced in the final reconstruction compromises the visibility of the microcalcifications, which cannot be distinguished from the background signal. Conversely, the optical tracking procedure (c) yields an image similar to the perfectly compensated displacement (b), restoring the calcification visibility as well as the sharpness of interfaces. This is also demonstrated by the line profiles measured across a microcalcification (indicated by the arrows) in panels (e) to (h). Specifically, it is shown that the microcalcification signal is to a great extent recovered thanks to the optical tracking, while its sharpness evaluated via Gaussian fitting (0.20 ± 0.02 mm at FWHM) is equivalent to both the motor corrected and the reference static cases. Conversely, if the image is not corrected, the microcalcification signal is comparable with image noise.

Moreover, as in the case of the breast specimen sample, the similarity to the reference image has been evaluated. SSIM and nMSE have been measured within the yellow dotted area in Figure 3d for motor-based correction, optical tracking correction, and no correction at all, against the reference motionless image. The plot in Figure 10 demonstrates that the optical tracking correction is slightly worse but comparable to the ideal case, representing a great improvement with respect to the uncorrected image.

4 | DISCUSSION

The presented results demonstrate that vertical respiration displacements in the mm range reduce dramatically the visibility of features as spiculations and microcalcifications, which are paramount in the clinical evaluation of bCT images. Specifically, oscillations with a realistic amplitude of 1 mm impair image quality, leading to a severe blurring, masking the microcalcifications and distorting the fibroglandular texture. On the other hand, the described synchrotron-based setup can tolerate displacements around 0.1 mm: this rather small value is naturally linked to the spatial resolution of the setup, which is higher than in hospital-based clinical scanners, rendering such system more sensitive to motion-related artifacts. Nonetheless, also conventional bCT systems, both with cone-beam and fan-beam spiral geometries, are capable of delivering high-resolution CT reconstructions with voxel sizes in the order of 150 μm cubed.[4,6] Moreover, the patient undergoing a hospital bCT scan is usually instructed to breathe normally,[6] as in synchrotron-based examinations. Thus, a typical 10 s long scan can record one to three respiratory cycles. For these reasons, although no dedicated study exists, also hospital-bCT systems may arguably be affected by motion artifacts due to involuntary movement, potentially causing a loss in the visibility of features which could otherwise be resolved. Moreover, the presence of motion artifacts could be even more relevant for novel functional breast imaging techniques, as 4D bCT, which has a duration longer than conventional bCT.[50-52]

In general, the adoption of strategies to prevent and/or compensate for involuntary motion appears to be

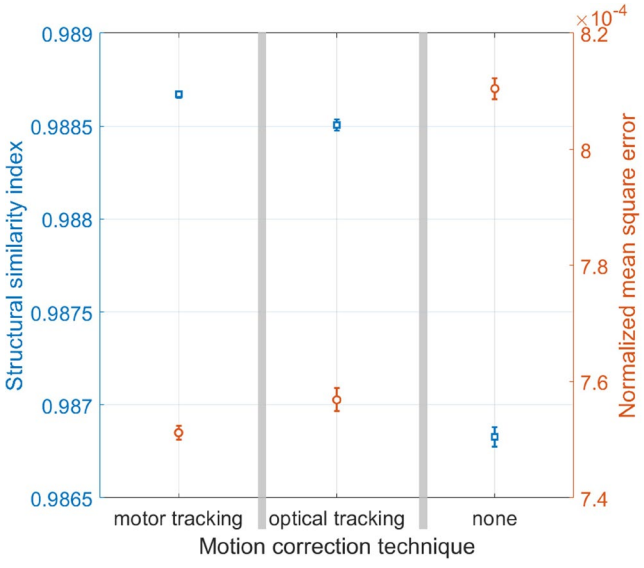

FIGURE 10 Plot displaying the structural similarity index (SSIM, blue curve and points) and the mean square error (nMSE, orange curve and points) as a function of the correction procedure. When not visible the error bars are smaller than the markers [Color figure can be viewed at wileyonlinelibrary.com]

mandatory for synchrotron-based setups and potentially useful also in hospital scanners. In this context, the optical tracking of fiducial marks positioned on the breast (phantom) surface is a very promising strategy to compensate for motion-related artifacts. Results show that, following a calibration procedure, optical tracking allows the restoration of image quality to levels comparable with the static reference image, recovering all the microcalcifications and introducing only a marginal blurring. While these findings have been proven only for synchrotron radiation bCT, it can be anticipated that optical tracking methods could be a viable solution for motion correction also in clinical bCT systems. In a realistic clinical scenario, the adoption of an optical tracking system would not have a relevant impact on the setup complexity and its implementation in the reconstruction workflow would not significantly increase the processing times as it only requires a translation of the projection images. Moreover, the optical tracking procedure can be coupled with the use of breast holding/constraining devices, whose role would be to limit large displacements of the breast while the tracking would compensate for subtle residual movements.

In particular, optical tracking can be taken into account when data-driven techniques, that is, methods relying on the acquired imaging data only, do not provide satisfactory results. On the other hand, the possibility to compensate for motion by exploiting only the acquired projection data is highly attractive both for synchrotron radiation and conventional bCT, as it would avoid the need for additional hardware and/or external data. Ideally, a method where the collection of additional imaging data is not required (such as e.g., a very fast scan before and/or after the actual acquisition) is desirable. Additional data acquisition could in fact be incompatible with *in vivo* imaging as an extra dose would be delivered to the patient and also, for the case of our synchrotron-based setup, could be technically challenging or unfeasible. Actually, advanced techniques for motion and also deformation compensation in CT have been proposed in recent years, within the community of high-resolution tomography with synchrotron radiation, to deal with sudden random motions of the sample during the scan.[27-30] However, the translation of such methods to bCT may not be straightforward. For instance, breast motion follows patient's respiration rate which is much lower than the detector frame rate. This results in very minor displacements which are hardly detectable on consecutive projection images. One more aspect to consider is that, in the specific case of synchrotron bCT with laminar x-ray beam, the field-of-view for each scan is much smaller than the whole organ, thus making the motion compensation via data-driven techniques even more challenging. It is not excluded, however, that future research activity will include refined image registration and processing solutions to enhance the accuracy of motion correction.

At this point, it should be stressed that the present study has been focused on the respiratory motion, which has been modeled as a rigid translation along the vertical axis. Of course, this is a rather simplified model which requires further refinements as the breast motion is in general more complex (non-rigid and along an arbitrary direction). For this reason a more sophisticated tracking setup will be implemented to monitor complex motion patterns (translations along y- and x-axis, plus angular tilts), which will be simulated with the hexapod motors.

5 | CONCLUSION

In the process of designing a bCT clinical protocol at the Elettra synchrotron in Trieste (Italy), crucial issues are related to the patient's respiratory motion. The present study aimed at assessing such motion, at evaluating the related artifacts, and at setting up a correction procedure by means of a custom optical tracking system. Typical movements were first assessed on seven volunteers, positioned on the patient's support at the SYRMEP beamline but not exposed to x-rays. Then, a similar motion was simulated during the CT scans of a breast tissue and a phantom, both acquired at 28 keV and with a glandular dose of 5 mGy. The motion of the breast phantom was faithfully registered through the optical tracking of fiducial marks. A quantitative analysis of the reconstructed CT images showed that, while residual motion of the order of one-tenth of millimeter (comparable with the system's point spread function) can be tolerated, larger movements have a critical impact on the visualization of spiculations and microcalcifications, and thus on the bCT diagnostic value. However, the correction procedure based on the optical tracking system was able to restore the pristine image quality, at a level comparable with the static reference. Even though the simulated movement was simplified, namely limited to the vertical direction, these results confirmed the idea that optical tracking can address the problem of motion artifacts. Further experiments are now scheduled to prove the validity of this approach for more realistic movements. Overall, our experience confirms that optical tracking motion correction is a valuable tool in synchrotron radiation bCT and suggests that it could be beneficial also in hospital bCT systems.

ACKNOWLEDGMENTS

The authors thank Prof. Kevin Charles Prince for proofreading the article. The authors acknowledge Euro-BioImaging (www.eurobioimaging.eu) for providing access to imaging technologies and services via the Phase Contrast Imaging Flagship Node (Trieste, Italy).

CONFLICT OF INTEREST

The authors have no conflict of interest to disclose.

DATA AVAILABILITY STATEMENT

Data are available from request to the authors.

REFERENCES

1. Lindfors KK, Boone JM, Nelson TR, Yang K, Kwan AL, Miller DF. Dedicated breast CT: initial clinical experience. *Radiology*. 2008;246:725-733.
2. O'Connell AM, Karellas A, Vedantham S. The potential role of dedicated 3D breast CT as a diagnostic tool: review and early clinical examples. *Breast J*. 2014;20:592-605.
3. Shah JP, Mann SD, McKinley RL, Tornai MP. Three dimensional dose distribution comparison of simple and complex acquisition trajectories in dedicated breast CT. *Med Phys*. 2015;42(8):4497-4510. http://dx.doi.org/10.1118/1.4923169
4. Wienbeck S, Lotz J, Fischer U. Review of clinical studies and first clinical experiences with a commercially available cone-beam breast CT in Europe. *Clin Imaging*. 2017;42:50-59.
5. O'Connell AM, Karellas A, Vedantham S, Kawakyu-O'Connor DT. Newer technologies in breast cancer imaging: dedicated cone-beam breast computed tomography. *Semin Ultrasound CT MRIno*. 2018;39:106-113 ; Elsevier.
6. Berger N, Marcon M, Saltybaeva N, et al. Dedicated breast computed tomography with a photon-counting detector: initial results of clinical in vivo imaging. *Invest Radiol*. 2019;54(7):409-418.
7. Vedantham S, Tseng H-W, Konate S, Shi L, Karellas A. Dedicated cone-beam breast CT using laterally-shifted detector geometry: quantitative analysis of feasibility for clinical translation. *J X-ray Sci Technol*. 2020;28(3):1-22.
8. Dullum JR, Lewis EC, Mayer JA. Rates and correlates of discomfort associated with mammography. *Radiology*. 2000;214:547-552.
9. Papas MA, Klassen AC. Pain and discomfort associated with mammography among urban low-income African-American women. *J Commun Health*. 2005;30:253-267.
10. Kalender WA, Kolditz D, Steiding C, et al. Technical feasibility proof for high resolution low-dose photon-counting CT of the breast. *Eur Radiol*. 2017;27:1081-1086.
11. Longo R, Arfelli F, Bellazzini R, et al. Towards breast tomography with synchrotron radiation at Elettra: first images. *Phys Med Biol*. 2016;61:1634.
12. Longo R, Arfelli F, Bonazza D, et al. Advancements towards the implementation of clinical phase-contrast breast computed tomography at Elettra. *J Synchr Radiat*. 2019;26:1343-1353.
13. Pacilé S, Brun F, Dullin C, et al. Clinical application of low-dose phase contrast breast CT: methods for the optimization of the reconstruction workflow. *Biomed Opt Expr*. 2015;6:3099-3112.
14. Gureyev T, Nesterets YI, Baran P, et al. Propagation-based x-ray phase-contrast tomography of mastectomy samples using synchrotron radiation. *Med Phys*. 2019;46:5478-5487.
15. Taba ST, Baran P, Nesterets YI, et al. Comparison of propagation-based CT using synchrotron radiation and conventional cone-beam CT for breast imaging. *Eur Radiol* 2020:1-11.
16. Bravin A, Coan P, Suortti P. X-ray phase-contrast imaging: from pre-clinical applications towards clinics. *Phys Med Biol*. 2012;58:R1.
17. Rigon L. X-ray imaging with coherent sources. *Comprehens Biomed Phys*. 2014;2:193-216.
18. Delogu P, Di Trapani V, Brombal L, Mettivier G, Taibi A, Oliva P. Optimization of the energy for breast monochromatic absorption X-ray Computed Tomography. *Sci Rep*. 2019;9(1). http://dx.doi.org/10.1038/s41598-019-49351-2
19. Fedon C, Rigon L, Arfelli F, et al. Dose and diagnostic performance comparison between phase-contrast mammography with synchrotron radiation and digital mammography: a clinical study report. *J Med Imaging*. 2018;5:13503.
20. Wilkins SW, Gureyev TE, Gao D, Pogany A, Stevenson AW. Phase-contrast imaging using polychromatic hard X-rays. *Nature*. 1996;384(6607):335-338. http://dx.doi.org/10.1038/384335a0
21. Paganin D, Mayo S, Gureyev TE, Miller PR, Wilkins SW. Simultaneous phase and amplitude extraction from a single defocused image of a homogeneous object. *J Microsc*. 2002;206:33-40.
22. Gureyev TE, Nesterets YI, Kozlov A, Paganin DM, Quiney HM. On the "unreasonable" effectiveness of transport of intensity imaging and optical deconvolution. *JOSA A*. 2017;34:2251-2260.
23. Brombal L, Donato S, Dreossi D, et al. Phase-contrast breast CT: the effect of propagation distance. *Phys Med Biol*. 2018;63(24):24NT03.
24. Brombal L, Arfelli F, Delogu P, et al. Image quality comparison between a phase contrast synchrotron radiation breast CT and a clinical breast CT: a phantom based study. *Sci Rep*. 2019;9:1-12.
25. Rößler A, Wenkel E, Althoff F, Kalender W. The influence of patient positioning in breast CT on breast tissue coverage and patient comfort. *Senologie-Zeitschrift für Mammadiagnostik und-therapie*. 2015;12:96-103.
26. Lewis SJ, Tam N, Pena LMA, et al. Getting a-breast of immobilisation needs for the implementation of phase contrast tomography. *Proc SPIE 11513, 15th International Workshop on Breast Imaging (IWBI2020)*. 2020;115131P. https://doi.org/10.1117/12.2563572
27. Dierksen K, Typke D, Hegerl R, Baumeister W. Towards automatic electron tomography II. *Implement Autof low-dose Proced Ultramicrosc*. 1993;49:109-120.
28. Guizar-Sicairos M, Diaz A, Holler M, et al. Phase tomography from x-ray coherent diffractive imaging projections. *Opt Expr*. 2011;19:21345-21357.
29. Gürsoy D, Hong YP, He K, et al. Rapid alignment of nanotomography data using joint iterative reconstruction and reprojection. *Sci Rep*. 2017;7:1-12.
30. Van Nieuwenhove V, De Beenhouwer J, De Schryver T, Van Hoorebeke L, Sijbers J. Data-driven affine deformation estimation and correction in cone beam computed tomography. *IEEE Trans Image Process*. 2017;26:1441-1451.
31. Brombal L, Golosio B, Arfelli F, et al. Monochromatic breast computed tomography with synchrotron radiation: phase-contrast and phase-retrieved image comparison and full-volume reconstruction. *J Med Imaging*. 2018;6(3):1. http://dx.doi.org/10.1117/1.jmi.6.3.031402
32. Fedon C, Longo F, Mettivier G, Longo R. GEANT4 for breast dosimetry: parameters optimization study. *Phys Med Biol*. 2015;60:N311.
33. Mettivier G, Fedon C, Di Lillo F, et al. Glandular dose in breast computed tomography with synchrotron radiation. *Phys Med Bio*. 2016;61(2):569-587. http://dx.doi.org/10.1088/0031-9155/61/2/569
34. Piai A, Contillo A, Arfelli F, et al. Quantitative characterization of breast tissues with dedicated CT imaging. *Phys Med Biol*. 2019;64:155011.
35. Brombal L. Effectiveness of X-ray phase-contrast tomography: effects of pixel size and magnification on image noise. *J Instrument*. 2020;15:C01005.
36. Delogu P, Golosio B, Fedon C, et al. Imaging study of a phase-sensitive breast-CT system in continuous acquisition mode. *J Instrument*. 2017;12:C01016.
37. Donato S, Brombal L, Tromba G, Longo R. Phase-contrast breast-CT: optimization of experimental parameters and reconstruction algorithms in world congress on medical physics and

biomedical engineering. *IFMBE Proceedings*. 2019;61:109-115; Springer.
38. Donato S, Brombal L, Arfelli F et al. Optimization of a customized Simultaneous Algebraic Reconstruction Technique algorithm for breast CT. In 2019 IEEE Nuclear Science Symposium and Medical Imaging Conference (NSS/MIC):1-2.
39. Contillo A, Veronese A, Brombal L, et al. A proposal for a quality control protocol in breast CT with synchrotron radiation. *Radiol Oncol*. 2018;52:329.
40. Tromba G, Longo R, Abrami A, et al. The SYRMEP Beamline of Elettra: clinical mammography and bio-medical applications. *AIP Conf Proc*. 2010;1266:18-23.
41. Castelli E, Tonutti M, Arfelli F, et al. Mammography with synchrotron radiation: first clinical experience with phase-detection technique. *Radiology*. 2011;259:684-694.
42. Mettivier G, Masi M, Arfelli F, et al. Radiochromic film dosimetry in synchrotron radiation breast computed tomography: a phantom study. *J Synchrotr Radiat*. 2020;27(3):762-771.
43. Oliva P, Di Trapani V, Arfelli F, et al. Experimental optimization of the energy for breast-CT with synchrotron radiation. *Sci Rep*. 2020;10:1-13.
44. Donato S, Arfelli F, Brombal L, et al. Flattening filter for Gaussian-shaped monochromatic X-ray beams: an application to breast computed tomography. *J Synchrotr Radiat*. 2020;27(2):503-506.
45. Bellazzini R, Spandre G, Brez A, Minuti M, Pinchera M, Mozzo P, Mozzo P. Chromatic X-ray imaging with a fine pitch CdTe sensor coupled to a large area photon counting pixel ASIC. *J Instrument*. 2013;8:C02028.
46. Delogu P, Oliva P, Bellazzini R, et al. Characterization of Pixirad-1 photon counting detector for X-ray imaging. *J Instrum*. 2016;11:P01015.
47. Brombal L, Donato S, Brun F, et al. Large-area single-photon-counting CdTe detector for synchrotron radiation computed tomography: a dedicated pre-processing procedure. *J Synchrotron Radiat*. 2018;25(4):1068-1077. http://dx.doi.org/10.1107/s1600577518006197
48. Brun F, Pacilè S, Accardo A, et al. Enhanced and flexible software tools for X-ray computed tomography at the Italian synchrotron radiation facility elettra. *Fundamenta Informaticae*. 2015;141(2-3):233-243. http://dx.doi.org/10.3233/fi-2015-1273
49. ZWang A, Bovik CH, Sheikh R, Simoncelli EP. Image quality assessment: from error visibility to structural similarity. *IEEE Trans Image Process*. 2004;13:600-612.
50. Prionas ND, Lindfors KK, Ray S, et al. Contrast-enhanced dedicated breast CT: initial clinical experience. *Radiology*. 2010;256:714-723.
51. Uhlig J, Fischer U, Surov A, Lotz J, Wienbeck S. Contrast-enhanced cone-beam breast-CT: analysis of optimal acquisition time for discrimination of breast lesion malignancy. *Eur J Radiol*. 2018;99:9-16.
52. Caballo M, Michielsen K, Fedon C, Sechopoulos I. Towards 4D dedicated breast CT perfusion imaging of cancer: development and validation of computer simulated images. *Phys Med Biol*. 2019;64:245004.

SUPPORTING INFORMATION

Additional supporting information may be found online in the Supporting Information section.

How to cite this article: Brombal L, Arana Peña LMA, Arfelli F, et al. Motion artifacts assessment and correction using optical tracking in synchrotron radiation breast CT. *Med Phys*. 2021;48:5343–5355. https://doi.org/10.1002/mp.15084